

Neutron scattering study of dipolar spin ice $\text{Ho}_2\text{Sn}_2\text{O}_7$: Frustrated pyrochlore magnet

Hiroaki Kadokawa

Department of Physics, Tokyo Metropolitan University, Hachioji-shi, Tokyo 192-0397, Japan

Yoshinobu Ishii

Advanced Science Research Center, Japan Atomic Energy Research Institute, Tokai, Ibaraki 319-1195, Japan

Kazuyuki Matsuhira* and Yukio Hinatsu

Division of Chemistry, Graduate School of Science, Hokkaido University, Sapporo, Japan

(received: May 21, 2001)

By means of neutron scattering techniques we have investigated the frustrated pyrochlore magnet $\text{Ho}_2\text{Sn}_2\text{O}_7$, which was found to show a ferromagnetic spin-ice behavior below $T \simeq 1.4$ K by susceptibility measurements. High-resolution powder-neutron-diffraction shows no detectable disorder of the lattice, which implies appearance of a random magnetic state solely by frustrated geometry, i.e., the corner sharing tetrahedra. Magnetic inelastic-scattering spectra show that Ho magnetic moments behave as an Ising spin system at low temperatures, and that the spin fluctuation has static character. The system remains in a short-range ordered state down to $T = 0.4$ K. By analyzing the wave-number dependence of the magnetic scattering using a mean field theory, it is clarified that the Ising spins interact via the dipolar interaction. Therefore we conclude that $\text{Ho}_2\text{Sn}_2\text{O}_7$ belongs to the dipolar-spin-ice family. Slow spin dynamics is exhibited as thermal hysteresis and time dependence of the magnetic scattering.

75.25.+z, 75.10.Hk, 75.50.Lk, 75.40.Gb

I. INTRODUCTION

Frustrated spin systems have been investigated mostly in antiferromagnets on geometrically frustrated lattices such as triangular, kagome, FCC, pyrochlore lattices. Recently an intriguing frustrated system was found in an Ising ferromagnet on the pyrochlore lattice by Harris *et al.*,^{1,2} where magnetic ions form a lattice of corner sharing tetrahedra illustrated in Fig. 1. When spins interact via a ferromagnetic nearest-neighbor exchange-interaction and have strong local Ising-anisotropies which force each spin to point into or out-of the center of each tetrahedron, spin configurations of the ground-state on one tetrahedron are sixfold degenerate “two-in and two-out” structures (see Fig. 1). By extending this “two-in-two-out” structure to the entire pyrochlore lattice, it was shown that ground state degeneracy is macroscopic, which leads to the residual entropy^{3,4} at $T = 0$. Since these spin configurations can be mapped to proton configurations in the cubic ice,³ the system is called as the spin ice model.^{1,2}

Recent discovery of spin-ice model systems, $\text{Ho}_2\text{Ti}_2\text{O}_7$ ^{1,5–10} and $\text{Dy}_2\text{Ti}_2\text{O}_7$,^{4,5} which belong to a series of pyrochlore oxides showing frustrated properties, has renewed interest of ice models. Experimental and theoretical work of these compounds has shown that the spin system freezes into a certain state below a temperature of the order $T = 1$ K^{1,8} which has only short range order^{1,2,9} with macroscopic number of degeneracy, i.e., zero-point entropy.^{3–5,11}

Although the strong Ising-like anisotropies of Ho and Dy moments are obvious, the spin-spin interactions have

certain ambiguity, because these large moments systems have significant contribution from dipolar interaction^{4,6} in addition to the nearest-neighbor exchange-interaction. The long-range nature of the dipolar interaction complicates the real spin-ice systems, and another theoretical problem of a dipolar spin-ice model^{11,12} has been addressed. The addition of the dipolar interaction removes the ground-state degeneracy and a long-range ordered state becomes the ground state. However experiments and Monte Carlo simulations do not show this magnetic order. This contradiction is thought to be solved by slow spin dynamics in the macroscopic number of low energy states belonging to the “two-in-two-out” manifold of the spin ice model, which prevents the dipolar spin ice from reaching to thermal equilibrium states.

Recently, other pyrochlore compounds $\text{Ho}_2\text{Sn}_2\text{O}_7$ and $\text{Dy}_2\text{Sn}_2\text{O}_7$ were shown to belong to the spin ice families by AC susceptibility measurements.⁸ It was shown that $\text{Ho}_2\text{Sn}_2\text{O}_7$ exhibits the slow dynamics below a temperature scale of $T_f \simeq 1.4$ K, and that it does not have a magnetic transition to a long-range ordered phase down to $T = 0.15$ K.

In this work, in order to clarify the spin ice behavior of $\text{Ho}_2\text{Sn}_2\text{O}_7$ on a microscopic basis, we have performed neutron scattering experiments on a powder sample. By measuring magnetic diffraction pattern down to $T = 0.4$ K, formation of magnetic short-range order and freezing effects were investigated. We analyzed the diffraction pattern using a mean field approximation of wave-number dependent susceptibilities, and evaluated inter-spin interaction constants. In addition, we measured magnetic inelastic-scattering spectra to elucidate

energy scales of spin fluctuations. Since a disorder of the pyrochlore lattice can influence the interpretation of experimental results in particular about the origin of the slow dynamics, we studied the crystal structure using high-resolution powder-neutron-diffraction.

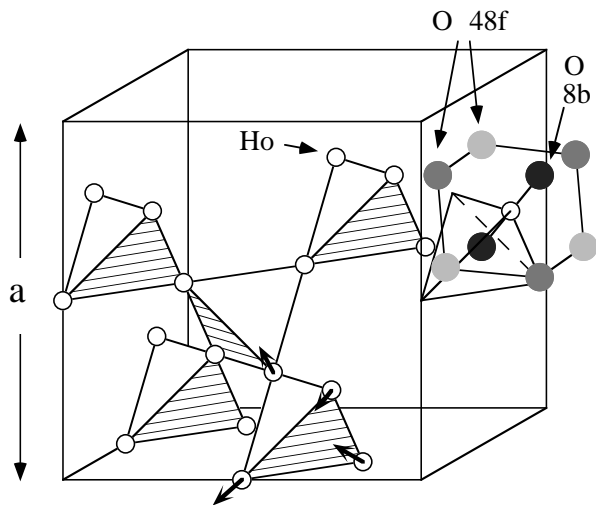


FIG. 1. Network of corner sharing tetrahedra of Ho is shown in a unit cell of the pyrochlore $\text{Ho}_2\text{Sn}_2\text{O}_7$. Oxygen atoms giving rise to local trigonal symmetry around a Ho atom, and “two-in-two-out” spin configuration on a tetrahedron are also illustrated.

II. EXPERIMENTAL METHOD

A polycrystalline sample of $\text{Ho}_2\text{Sn}_2\text{O}_7$ was prepared by standard solid-state reaction.⁸ Stoichiometric mixture of Ho_2O_3 and SnO_2 was heated in air at $1200 - 1400^\circ\text{C}$ for 3 days with intermediate regrinding to ensure a complete reaction. The powder x-ray diffraction pattern of the sample indicates that it is a single phase with the cubic pyrochlore structure.

Neutron scattering experiments on the polycrystalline sample were performed using triple-axis spectrometers C11-HER and 4G-GPTAS installed at JRR-3M JAERI (Tokai). Incident or final neutron energies were fixed at 3 or 14 meV using the pyrolytic-graphite (002) monochromator or analyzer. Higher-order neutrons were removed by the cooled Be filter or the pyrolytic-graphite filter. The sample was mounted in a liquid ${}^3\text{He}$ cryostat or a closed cycle ${}^4\text{He}$ -gas refrigerator. A powder-diffraction experiment was carried out using the high-resolution powder-neutron-diffractometer (HRPD) installed at JRR-3M. Neutrons of the wave length $\lambda = 1.8238 \text{ \AA}$ were selected by the Ge (331) monochromator.

III. EXPERIMENTAL RESULTS

A. Crystal structure

The crystal structure of $\text{Ho}_2\text{Sn}_2\text{O}_7$ was studied by x-ray diffraction.⁸ It was shown that the powder pattern is consistent with the fully ordered cubic pyrochlore structure. This structure belongs to the space group $Fd\bar{3}m$ (No. 227), and constituent atoms fully occupy the sites of $16d(\text{Ho})$, $16c(\text{Sn})$, $48f(\text{O})$, and $8b(\text{O}')$.¹³ To confirm this more precisely and detect certain randomness in the lattice, we measured a powder-neutron-diffraction pattern at a room temperature. The observed pattern is shown in Fig. 2. This was analyzed by using the Rietveld profile refinement program RIETAN-97.¹⁴ We performed the profile fitting first by assuming the fully ordered pyrochlore structure. The resulting structure parameters are listed in Table I, and the fitted powder pattern and the difference curve are shown in Fig. 2. From this figure and the final R factors of $R_{\text{wp}} = 7.8\%$ ($R_{\text{e}} = 6.4\%$), $R_{\text{p}} = 5.8\%$ and $R_{\text{B}} = 3.5\%$, we conclude that the quality of the fit is excellent.

This refinement suggests that we do not need to introduce any randomness of the lattice to improve the refinement, or that the experimental data do not contain enough information to pursue small deviation from the pyrochlore structure. Thus we checked only one possibility which is commonly observed in oxides, that is, deficiency of oxygen atoms. A profile fitting with adjustable occupation parameters of $48f(\text{O})$ and $8b(\text{O}')$ sites was carried out. The consequent occupations were $n(48f) = 1.00(3)$ and $n(8b) = 0.93(7)$. This implies that determination of the oxygen deficiency from the present powder diffraction data is rather limited. We note in particular that since the $8b(\text{O}')$ site oxygen is located at the center of the tetrahedron (see Fig. 1), small amount of deficiency of this oxygen might substantially affect the Ising anisotropy of the Ho spin. Although more precise measurements or different techniques are required to examine small randomness, we conclude that the present diffraction data are consistent with the fully ordered pyrochlore structure.

TABLE I. Refined structure parameters of $\text{Ho}_2\text{Sn}_2\text{O}_7$ at $T = 290 \text{ K}$ using fully ordered pyrochlore structure. Number in parenthesis is standard deviation of the last digit.

$Fd\bar{3}m$ (No. 227) $a = 10.381(1) \text{ \AA}$					
Atom	Site	x	y	z	$B (\text{\AA}^2)$
Ho	$16d$	$1/2$	$1/2$	$1/2$	$0.3(2)$
Sn	$16c$	0	0	0	$0.3(2)$
O	$48f$	$0.3368(5)$	$1/8$	$1/8$	$0.5(1)$
O'	$8b$	$3/8$	$3/8$	$3/8$	$0.3(3)$

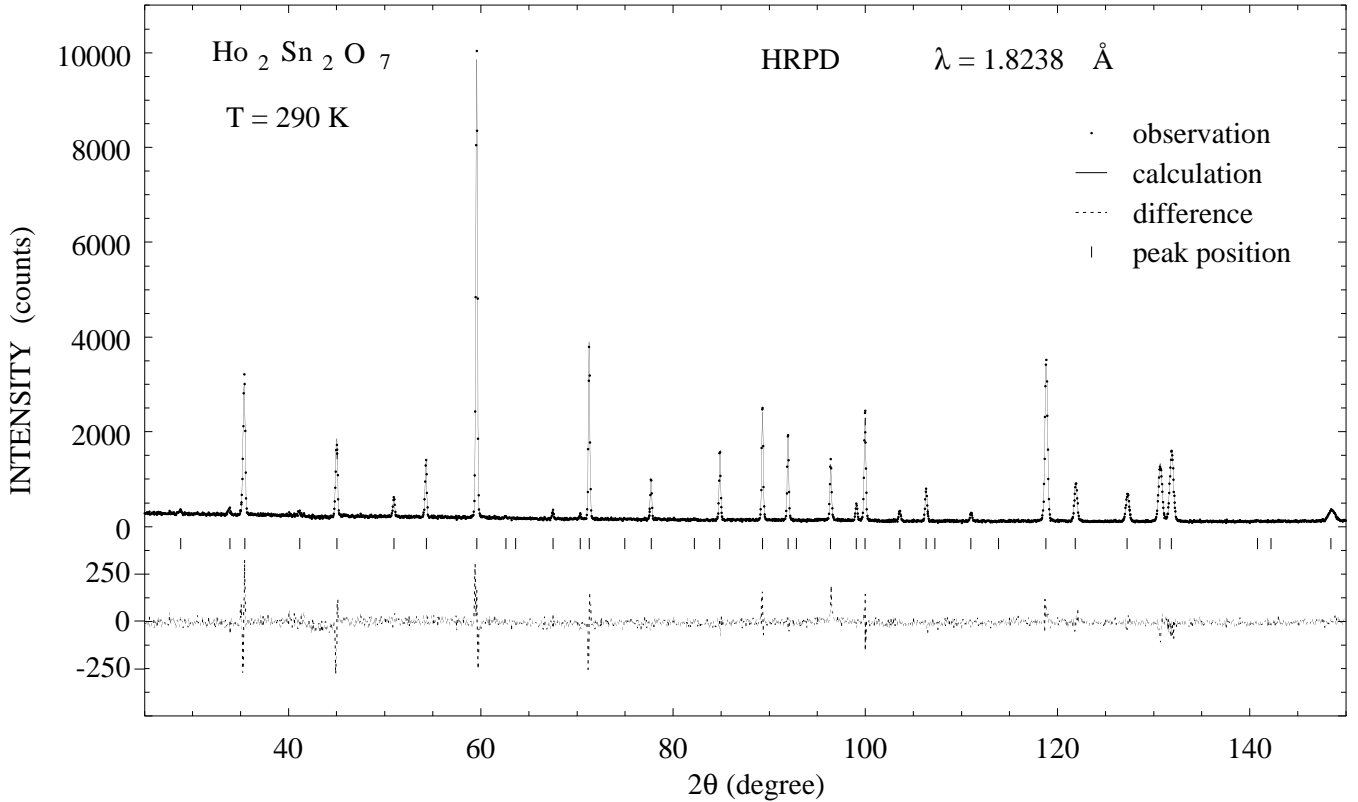


FIG. 2. Neutron diffraction pattern of $\text{Ho}_2\text{Sn}_2\text{O}_7$ measured at $T = 290$ K. Observed and calculated patterns are denoted by closed circles and solid line, respectively. Their difference is plotted in lower part by dashed line. Vertical bars stand for positions of Bragg reflections.

B. Magnetic excitation

Magnetic excitation spectra were measured to examine characteristic energy scales of magnetic fluctuations at low temperatures and crystal field excitations. In Fig. 3(a) we show excitation spectra in a low energy range $-1 < E < 7$ meV measured using the C11 spectrometer with a condition of the horizontal focusing analyzer with $E_f = 3.1$ meV. The excitation peaks observed at $T = 80$ K are transitions between crystal-field energy levels excited thermally. Below $T = 40$ K they almost vanish because of negligible thermal occupations, and magnetic signals are observed only near the elastic channel. A few typical energy scans near $E = 0$ are shown in Fig. 3(b). By fitting these peaks to the Gaussian form, we obtained energy widths of $\Delta E_{\text{FWHM}} = 83 \pm 8$, 84 ± 8 , and 88 ± 8 μeV as shown in the figure. Since these values are in agreement with the energy resolution $\Delta E_{\text{FWHM}} = 85$ μeV measured using the standard vanadium, we conclude that the magnetic signal near $E = 0$ do not show any intrinsic inelasticity within the present experimental condition. The upper limit of the intrinsic energy width is $\Delta E_{\text{FWHM}} < 30$ μeV , which is 0.3 K in the temperature scale. These observations are consistent with the strong Ising anisotropy of the spin system.

The crystal-field excitation spectra were measured in a wider energy range using the 4G spectrometer with a

condition $E_f = 14$ meV. In Fig. 4 energy scans in a range $5 < E < 30$ meV at $Q = 2 \text{ \AA}^{-1}$ are shown. One can see clearly that there are two excitation peaks at $E = 22$ and 26 meV. Temperature variation of the spectra elucidates magnetic origin of these peaks. The positions of these crystal-field excitations coincide with those observed in the similar compound $\text{Ho}_2\text{Ti}_2\text{O}_7$.^{7,6} For $\text{Ho}_2\text{Ti}_2\text{O}_7$ the crystal-field state has been thoroughly studied by neutron inelastic scattering, and the strong Ising character of the ground doublet is established.⁷ Because of similarity between the Ti- and Sn- compounds, we may conclude that the ground doublet of $\text{Ho}_2\text{Sn}_2\text{O}_7$ has also the strong Ising anisotropy along the local $\langle 111 \rangle$ axes and it behaves as an Ising model at low temperatures.

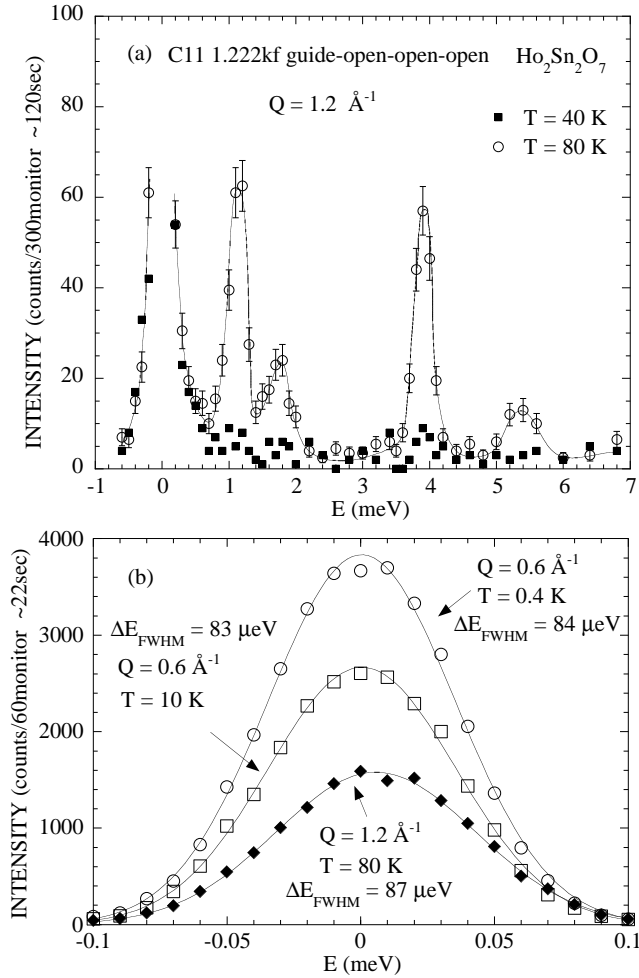


FIG. 3. (a) Spectrum of energy scan of $\text{Ho}_2\text{Sn}_2\text{O}_7$ measured at $T = 40$ and 80 K in range $-1 < E < 7 \text{ meV}$. Solid line is guide to the eye. (b) Detail of typical elastic scattering peaks for $0.4 < T < 80 \text{ K}$. Solid lines represent fits to the Gaussian function. Scans of (a) and (b) were carried out using the horizontally focusing analyzer with $E_f = 3.1 \text{ meV}$.

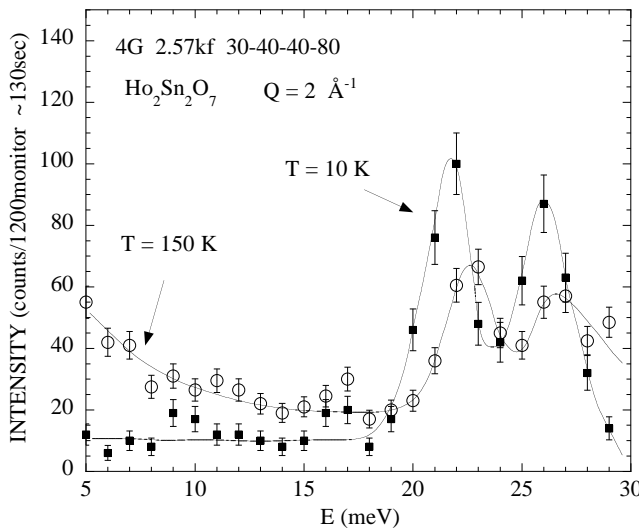


FIG. 4. Crystal-field excitation spectrum of $\text{Ho}_2\text{Sn}_2\text{O}_7$ measured at $Q = 2 \text{ \AA}^{-1}$ in energy range $5 < E < 30 \text{ meV}$. Solid lines are guides to the eye.

C. Magnetic elastic scattering

In the low temperature range where the system can be regarded as an Ising model, we studied magnetic short-range order, or spin correlation. As shown in Sec. III B the magnetic excitation spectra are completely elastic in the present experimental condition. In this case, double-axis data $\frac{d\sigma}{d\Omega}(\mathbf{Q})$ can be measured by triple-axis Q -scans with $E = 0$, which can be interpreted as the Fourier transform of the spin-pair correlation because the quasi-elastic approximation is applicable. We carried out Q -scans with elastic condition $E = 0$ using the C11 spectrometer at several temperatures down to $T = 0.4 \text{ K}$. The results of the Q -scans are shown in Fig. 5. One can see from this figure that the magnetic short-range order starts to develop below $T < 20 \text{ K}$. Although this energy scale is remarkably larger than the Curie-Weiss temperature $\theta_{\text{CW}} = 1.8 \text{ K}$, it is comparable to the blocking energy $E_B = 20 \text{ K}$.⁸ By analyzing the Q -dependence of the intensity, which will be explained in the next section, we obtained convincing evidence that the dipolar interaction is the major inter-spin coupling.

The temperature dependence of the scattering intensity at two typical wave numbers $Q = 0.59$ and 0.21 \AA^{-1} was measured in cooling and heating conditions, and is plotted in Fig. 6. We note that $Q = 0.21 \text{ \AA}^{-1}$ is the wave number where the largest variation of the intensity was observed at low temperatures. These data clearly demonstrate existence of thermal hysteresis of the magnetic scattering below $T_f \simeq 1.4 \text{ K}$. This temperature is in good agreement with the onset of the slow spin dynamics found by the AC susceptibility.⁸ The thermal hysteresis synonymously implies time dependence of the intensity. This time dependence was really observed as shown in the inset of Fig. 6. The scattering intensity at $Q = 0.21 \text{ \AA}^{-1}$ varies in the time scale of the order of ten minutes, after the temperature is cooled to $T = 0.4 \text{ K}$. From these experimental facts we conclude that the onset of the slow spin dynamics in $\text{Ho}_2\text{Sn}_2\text{O}_7$ is slow formation of the short range order.

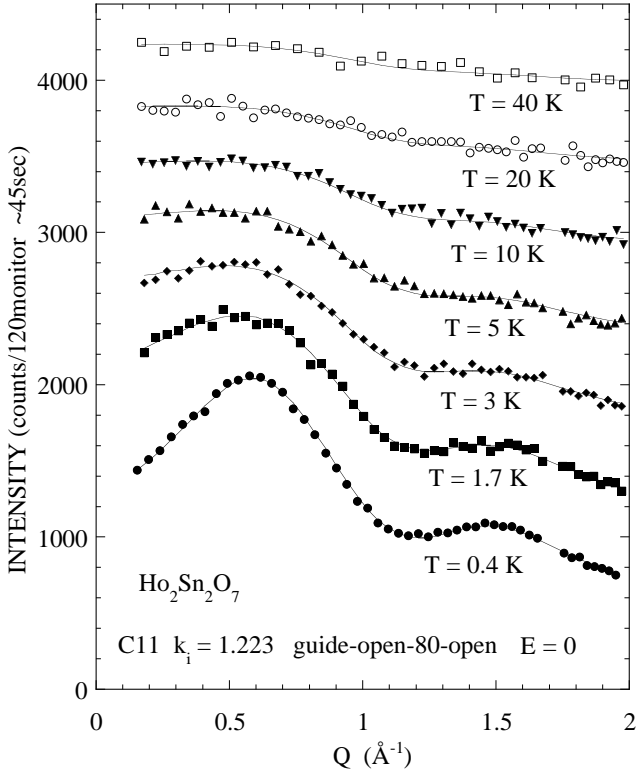


FIG. 5. Elastic magnetic scattering of $\text{Ho}_2\text{Sn}_2\text{O}_7$ as a function of wave number at various temperatures. Data of $T = 1.7, 3, 5, 10, 20$, and 40 K are shifted by 500, 1000, 1500, 2000, 2500, and 3000 counts, respectively for clarity. Solid lines are fitted curves calculated using Eqs. (4.11) and (4.12) of the mean field theory.

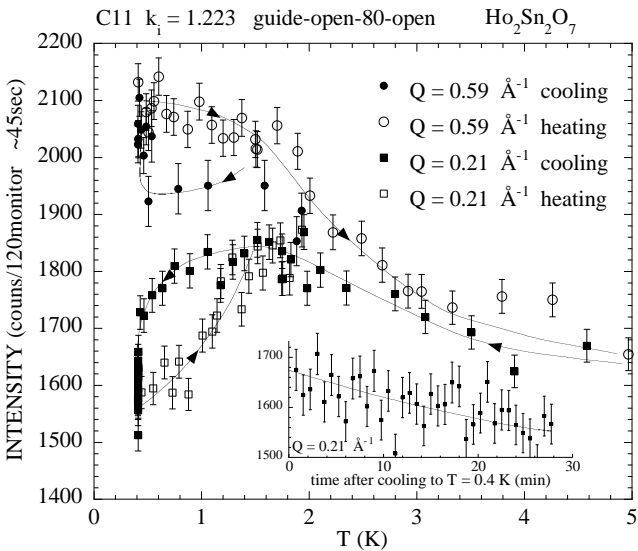


FIG. 6. Temperature dependence of elastic magnetic scattering of $\text{Ho}_2\text{Sn}_2\text{O}_7$ measured at $Q = 0.59$ and 0.21 \AA^{-1} in cooling and heating conditions. The inset shows time dependence of intensity at $Q = 0.21$ \AA^{-1} after temperature is cooled to $T = 0.4$ K. Solid lines are guides to the eye.

IV. MEAN FIELD ANALYSIS OF MAGNETIC ELASTIC SCATTERING

A. Mean field theory

By analyzing the neutron scattering intensity $\frac{d\sigma}{d\Omega}(\mathbf{Q})$, it is possible to extract information of the magnetic interaction parameters. The simplest method to perform this is to utilize a mean field approximation of wave-number dependent susceptibilities.^{15,16} For simplicity of handling equations, we assume a spin Hamiltonian of a quadratic form of spins

$$H = - \sum_{n,\nu,\alpha,n',\nu',\beta} J_{n,\nu,\alpha;n',\nu',\beta} S_{n,\nu,\alpha} S_{n',\nu',\beta}, \quad (4.1)$$

where $S_{n,\nu,\alpha}$ represents α -component ($\alpha = x, y, z$) of a classical vector spin $\mathbf{S}_{n,\nu} = \mathbf{S}_{\mathbf{t}_n + \mathbf{d}_\nu}$ ($|\mathbf{S}_{n,\nu}| = 1$) on a ν -th site \mathbf{d}_ν ($\nu = 1, 2, 3, 4$) in an n -th chemical unit-cell located at \mathbf{t}_n . We further assume

$$\begin{aligned} H = & -D_a \sum_{n,\nu} \left[(\mathbf{n}_\nu \cdot \mathbf{S}_{n,\nu})^2 - |\mathbf{S}_{n,\nu}|^2 \right] \\ & - J_1 \sum_{\langle n,\nu;n',\nu' \rangle} \mathbf{S}_{n,\nu} \cdot \mathbf{S}_{n',\nu'} \\ & + D_{dp} r_{nn}^3 \sum_{\langle n,\nu;n',\nu' \rangle} \left[\frac{\mathbf{S}_{n,\nu} \cdot \mathbf{S}_{n',\nu'}}{|\mathbf{r}_{n,\nu;n',\nu'}|^3} \right. \\ & \left. - \frac{3(\mathbf{S}_{n,\nu} \cdot \mathbf{r}_{n,\nu;n',\nu'}) (\mathbf{S}_{n',\nu'} \cdot \mathbf{r}_{n,\nu;n',\nu'})}{|\mathbf{r}_{n,\nu;n',\nu'}|^5} \right], \end{aligned} \quad (4.2)$$

where

$$\mathbf{r}_{n,\nu;n',\nu'} = \mathbf{t}_n + \mathbf{d}_\nu - \mathbf{t}_{n'} - \mathbf{d}_{\nu'}. \quad (4.3)$$

The first term is the single-ion anisotropy energy with the local easy-axis direction \mathbf{n}_ν ($|\mathbf{n}_\nu| = 1$). To reproduce the strong Ising anisotropy we chose a large positive value $D_a = 810$ K. This value is rather arbitrary and other choices of $D_a = 1620$ or 405 K were confirmed not to change the following numerical results. The second term is the nearest-neighbor exchange-interaction, which has to be extended to further neighbors if it is required. The third term is the dipolar interactions of the Ho magnetic moments $\mu \mathbf{S}_{n,\nu}$, where μ is the magnitude of the moment $\mu \simeq g\sqrt{J(J+1)}\mu_B \simeq 10 \mu_B$. The interaction constant is $D_{dp} = \mu^2/r_{nn}^3 \simeq 1.4$ K, where $r_{nn} = a/(2\sqrt{2})$ is the distance between two nearest-neighbor spins. The dipolar energy between two nearest-neighbor spins¹¹ is $D_{nn} = 5D_{dp}/3 \simeq 2.4$ K.

Mean field theories of magnetic ordering and wave-number dependent susceptibilities are described in standard literature for a Bravais lattice.^{15,16} Extending this to a non-Bravais lattice is a little complicated but straightforward. Applications to pyrochlore magnets for magnetic ordering are described in Refs. 12,17, and 18.

In the mean field theory, the magnetic structure is determined by the Fourier transform of the interaction constants

$$J_{\mathbf{q};\nu,\alpha;\nu',\beta} = \sum_n J_{n,\nu,\alpha;n',\nu',\beta} \times \exp[-i\mathbf{q} \cdot (\mathbf{t}_n + \mathbf{d}_\nu - \mathbf{t}_{n'} - \mathbf{d}_{\nu'})], \quad (4.4)$$

where \mathbf{q} is a wave vector in the first Brillouin zone, and eigenvalue equations

$$\sum_{\nu',\beta} J_{\mathbf{q};\nu,\alpha;\nu',\beta} u_{\mathbf{q};\nu',\beta}^{(\rho)} = \lambda_{\mathbf{q}}^{(\rho)} u_{\mathbf{q};\nu,\alpha}^{(\rho)}. \quad (4.5)$$

The eigenvalues $\lambda_{\mathbf{q}}^{(\rho)}$ ($\rho = 1, 2, \dots, 12$) and the eigenvectors $u_{\mathbf{q};\nu,\alpha}^{(\rho)}$ were calculated by numerical diagonalization of the 12-dimensional real symmetric-matrix $J_{\mathbf{q};\nu,\alpha;\nu',\beta}$ ¹⁹ with the normalization condition

$$\sum_{\nu,\alpha} u_{\mathbf{q};\nu,\alpha}^{(\rho)} u_{\mathbf{q};\nu,\alpha}^{(\sigma)*} = \delta_{\rho,\sigma}. \quad (4.6)$$

The system first undergoes a phase transition to a long-range ordered phase at a temperature T_C , determined by

$$k_B T_C = \frac{2}{3} [\lambda_{\mathbf{q}}^{(\rho)}]_{\max(\mathbf{q},\rho)}, \quad (4.7)$$

where $[\dots]_{\max(\mathbf{q},\rho)}$ indicates a global maximum for all \mathbf{q} and ρ . The ordered magnetic structure is expressed by

$$\langle S_{n,\nu,\alpha} \rangle = \langle S_{\mathbf{q}}^{(\rho)} \rangle u_{\mathbf{q};\nu,\alpha}^{(\rho)} \exp[i\mathbf{q} \cdot (\mathbf{t}_n + \mathbf{d}_\nu)] + \text{c.c.}, \quad (4.8)$$

where $\langle S_{\mathbf{q}}^{(\rho)} \rangle$ is the amplitude of the modulation.

Wave-number dependent susceptibilities^{15,16} in the paramagnetic phase $T > T_C$ extended for non-Bravais lattices are defined by

$$\chi_{\mathbf{q};\nu,\alpha;\nu',\beta} = \frac{N^2 \mu^2}{V k_B T} \langle S_{-\mathbf{q};\nu',\beta} S_{\mathbf{q};\nu,\alpha} \rangle, \quad (4.9)$$

where N and V are a number of the unit cell and volume of the system, and

$$S_{\mathbf{q};\nu,\alpha} = \frac{1}{N} \sum_n S_{n,\nu,\alpha} \exp[-i\mathbf{q} \cdot (\mathbf{t}_n + \mathbf{d}_\nu)]. \quad (4.10)$$

In the mean field approximation, the wave-number dependent susceptibilities are calculated by using the eigenvalues and eigenvectors

$$\chi_{\mathbf{q};\nu,\alpha;\nu',\beta} = \frac{N \mu^2}{V} \sum_{\rho} \frac{u_{\mathbf{q};\nu,\alpha}^{(\rho)} u_{\mathbf{q};\nu',\beta}^{(\rho)*}}{3k_B T_{\text{MF}} - 2\lambda_{\mathbf{q}}^{(\rho)}}, \quad (4.11)$$

where T_{MF} is the temperature defined in the mean field approximation. Using this $\chi_{\mathbf{q};\nu,\alpha;\nu',\beta}$ the neutron scattering cross-section in the quasielastic approximation^{15,16} is expressed as

$$\frac{d\sigma}{d\Omega}(\mathbf{Q} = \mathbf{G} + \mathbf{q}) = C f(\mathbf{Q})^2 k_B T \sum_{\alpha,\beta,\nu,\nu'} \left(\delta_{\alpha\beta} - \hat{Q}_\alpha \hat{Q}_\beta \right) \times \chi_{\mathbf{q};\nu,\alpha;\nu',\beta} \cos[\mathbf{G} \cdot (\mathbf{d}_\nu - \mathbf{d}_{\nu'})], \quad (4.12)$$

where \mathbf{G} , C and $f(\mathbf{Q})$ stand for a reciprocal lattice vector, a constant, and a magnetic form factor, respectively.

B. Application to $\text{Ho}_2\text{Sn}_2\text{O}_7$

In order to estimate interaction constants from the observed intensity data shown in Fig. 5, we used Eqs. (4.11) and (4.12) as an experimental trial function, and performed least square fitting. In this fitting, C in Eq. (4.12) is treated as an adjustable scale factor of the intensity, because the sum rule of the cross-section, which is always satisfied experimentally, is violated for the theoretical equations (4.11) and (4.12). The temperature T_{MF} of Eq. (4.11) is also one of fitting parameters, and has little meaning as real temperature, especially in low temperatures where spin correlation is not negligible. If the intensity data at various temperatures are reproduced by the same interaction constants, we can think that the interaction constants obtained by this method have real physical meaning. We note that an obvious advantage of this analysis is simplicity, and that another advantage is numerical flexibility that any observed intensity data can be reproduced by introducing enough number of interaction constants.

To illustrate the theoretical scattering profile and to gain insight to what extent information can be extracted from the powder diffraction data, we calculated examples of the mean field $\frac{d\sigma}{d\Omega}(\mathbf{Q})$ in three limiting cases: spins interact only via (1) dipolar interaction $D_{\text{dp}} = 1.4$ K, $J_1 = 0$; (2) ferromagnetic nearest-neighbor exchange-interaction $J_1 = 2$ K, $D_{\text{dp}} = 0$; (3) antiferromagnetic nearest-neighbor exchange-interaction $J_1 = -2$ K, $D_{\text{dp}} = 0$. These three examples with certain values of T_{MF} and C are shown in Fig. 7. By comparing these curves with the observed data in Fig. 5, we may conclude that the observation excludes possibilities of the purely ferromagnetic or antiferromagnetic exchange-interaction and that the dipolar interaction and a small exchange interaction will account for the observation.

Along this line we fitted the experimental data at $T = 0.4$ K to the mean field expressions Eqs. (4.11) and (4.12) with fixed $D_{\text{dp}} = 1.4$ K and adjustable parameters of J_1 , T_{MF} and the intensity scale factor. The fitted values are $J_1 = 1.0 \pm 0.5$ K (ferromagnetic) and $T_{\text{MF}} = 2.2 \pm 0.1$ K. The calculated curve using the fitted parameters is plotted by the solid line in Fig. 5, which shows very good agreement. It should be noted that the large error of J_1 indicates that the diffraction pattern is almost reproduced only by the dipole interaction and that the small discrepancy of the fitting is improved by adding small contribution due to J_1 . By using this value $J_1 = 1.0$ K, we tried to fit other scattering data above $T > 0.4$ K with

the adjustable parameters of T_{MF} and the intensity scale factor. The resulting fit curves are shown by solid lines in Fig. 5. The excellent fit quality ensures that the relative strength of the dipolar and the exchange interactions is well established by the present analysis. In Fig. 8 the fitted values of T_{MF} are shown, which seems to have little meaning as expected. By following Ref. 11, we calculate the exchange energy between two nearest-neighbor spins $J_{\text{nn}} = \frac{1}{3}J_1 = 0.3 \pm 0.15$ K. This is 14 % of the dipolar energy $D_{\text{nn}} = 2.4$ K of two nearest-neighbor spins. Therefore we conclude that the major spin-spin coupling in $\text{Ho}_2\text{Sn}_2\text{O}_7$ is the dipolar interaction.

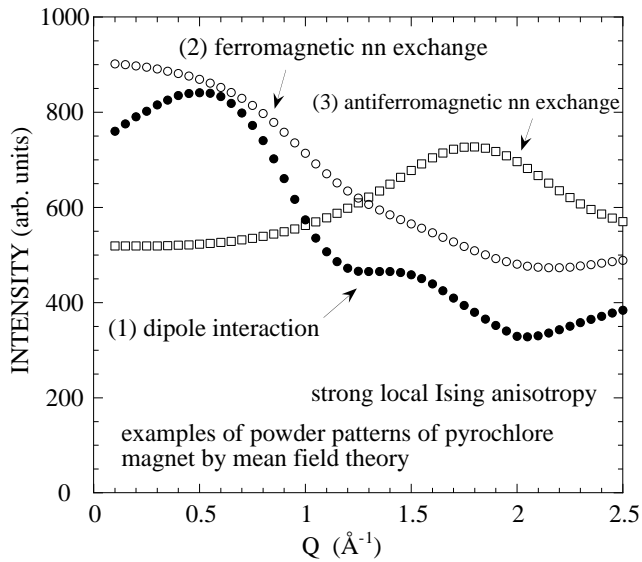


FIG. 7. Examples of magnetic scattering calculated using Eqs. (4.11) and (4.12) of the mean field theory. Spin interactions of three curves are (1) dipolar interaction $D_{\text{dp}} = 1.4$ K, $J_1 = 0$; (2) ferromagnetic nearest-neighbor exchange-interaction $J_1 = 2$ K, $D_{\text{dp}} = 0$; (3) antiferromagnetic nearest-neighbor exchange-interaction $J_1 = -2$ K, $D_{\text{dp}} = 0$.

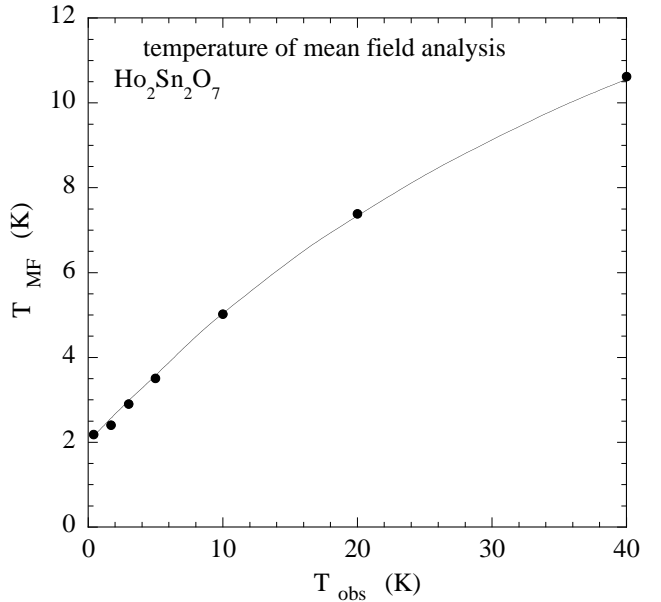


FIG. 8. Fitted values of the temperature of the mean field theory T_{MF} in Eq. (4.11) is plotted as a function of the observed temperature T_{obs} . Line is guide to the eye.

V. DISCUSSION

As shown in the previous section, the analysis of the magnetic interactions using the mean field theory in the paramagnetic phase seems successful from a view point of the experimental fitting. However applicability of the mean field theory has to be justified theoretically. In a high temperature range, Eq. (4.11) can be justified as an approximation to a high temperature expansion. On the other hand, in a low temperature range of the order $\theta_{\text{CW}} = 1.8$ K, the justification is less clear. Equation (4.11) may still be regarded as an approximation with a strongly renormalized temperature parameter T_{MF} , or may completely lose physical meaning. The experimental analysis suggests correctness of the former possibility. At present, we think at least, the conclusion that the main spin-spin interaction is the dipolar coupling will not be changed, when a more precise theoretical analysis is made. It should be noted that a recent neutron scattering work on a single-crystal $\text{Ho}_2\text{Ti}_2\text{O}_7$ elucidated dipolar nature of the spin interactions by using a Monte Carlo simulation analysis.⁹ We also obtained the same conclusion by using the present mean field analysis on another single-crystal neutron-data of $\text{Ho}_2\text{Ti}_2\text{O}_7$.¹⁰

For completeness of the mean field theory and the convenience for a reader, we would like to make a few comments on the long range order of Eqs. (4.8) and (4.7). The maximum eigenvalue $[\lambda_{\mathbf{q}}^{(\rho)}]_{\text{max}(\mathbf{q}, \rho)}$ is doubly degenerate at each \mathbf{X} point, $\mathbf{q} = \mathbf{a}^*, \mathbf{b}^*, \text{ or } \mathbf{c}^*$.²⁰ These wave numbers correspond to the peak position $Q \simeq 0.6 \text{ Å}^{-1} \simeq |(001)|$ of the Q -scan in Fig. 5. Using the corresponding

eigenvector $u_{\mathbf{q};\nu,\alpha}^{(\rho)}$, we depict a magnetic structure with $\mathbf{q} = \mathbf{c}^*$ in Fig. 9, which is also one of the ground states.²¹

A characteristic spin ice behavior observed in $\text{Ho}_2\text{Sn}_2\text{O}_7$ is the slow spin dynamics or a sort of spin freezing below $T_f \simeq 1.4$ K, which was found by the AC susceptibility measurements.⁸ Quite consistent behavior is observed by the present work as the thermal hysteresis and the time dependence of the magnetic scattering. This implies very slow development of the short range order. From these experimental facts, a natural question arises whether there exists a spin-glass phase-transition around T_f or around lower $T_m \simeq 0.75$ K which was defined by the onset of irreversibility of magnetization process,⁸ or it is interpreted as a blocking phenomenon. Since the nature of T_f nor T_m is not well understood, the question is to be answered by further studies. We note that the thermal hysteresis and the time dependence of the magnetic scattering was observed in a spin glass system.²²

According to the Monte Carlo simulation study of the dipolar spin-ice model,¹¹ the spin ice behavior occurs in a wide range of the interaction ratio $-0.8 < J_{nn}/D_{nn}$. The isomorphic systems $\text{Dy}_2\text{Ti}_2\text{O}_7$ and $\text{Ho}_2\text{Ti}_2\text{O}_7$ have small antiferromagnetic exchange-interactions with $J_{nn}/D_{nn} = -0.52$ and -0.22 , respectively.^{11,9} $\text{Ho}_2\text{Sn}_2\text{O}_7$ with $J_{nn}/D_{nn} = 0.14 \pm 0.07$ also belongs to this family.

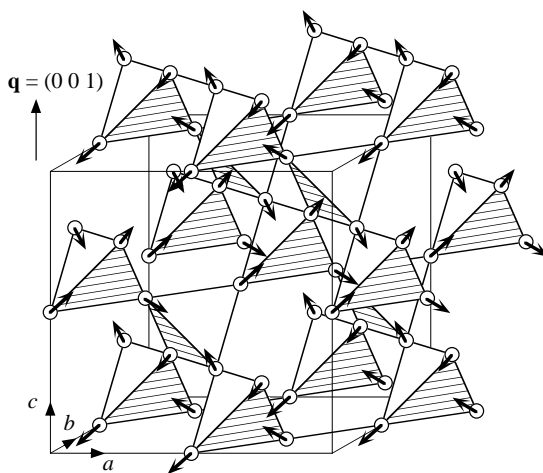


FIG. 9. Magnetic structure with modulation $\mathbf{q} = \mathbf{c}^*$ determined by Eqs. (4.7) and (4.8) of the mean field theory. This is also a ground-state spin-configuration of the dipolar spin-ice model.

VI. CONCLUSION

We have investigated the frustrated pyrochlore magnet $\text{Ho}_2\text{Sn}_2\text{O}_7$ by means of neutron scattering techniques using the powder sample. The high-resolution powder-diffraction shows that the crystal structure is the fully ordered pyrochlore structure with no detectable disorder. Because of the limitation of the present powder-diffraction data, possibilities of small amount of disorders

are to be studied. Magnetic excitation spectra demonstrate that the magnetic fluctuation is almost static at low temperatures below $T < 40$ K, in which the system behaves as an Ising model. The crystal-field excitations observed at $E = 22$ and 26 meV strongly suggest that the crystal-field state of $\text{Ho}_2\text{Sn}_2\text{O}_7$ is almost the same as that of the isomorphic Ising system $\text{Ho}_2\text{Ti}_2\text{O}_7$. By measuring elastic magnetic scattering at low temperatures down to $T = 0.4$ K, we observed only the short range order, which develops below $T < 20$ K. The wave-number dependence of the magnetic scattering has been analyzed successfully using the mean field theory. This analysis shows that spins interact mainly via the dipolar interaction and via the small additional nearest-neighbor exchange-interaction. Therefore we conclude that $\text{Ho}_2\text{Sn}_2\text{O}_7$ belongs to the dipolar-spin-ice family compounds. The spin freezing below $T_f \simeq 1.4$ K is observed as the thermal hysteresis and the time dependence of the magnetic scattering. This means unusual slow development of the short range order, which should be studied by future work.

ACKNOWLEDGMENTS

We would like thank M. Kanada, K. Motoya, M. Mekata, M. Sato, T. Sato, Y. Yasui for valuable discussions.

* Present address: Department of Electronics, Faculty of Engineering, Kyushu Institute of Technology, Kitakyushu 804-8550, Japan.

¹ M. J. Harris, S. T. Bramwell, D. F. McMorrow, T. Zeiske, and K. W. Godfrey, Phys. Rev. Lett. **79**, 2554 (1997).

² S. T. Bramwell and M. J. Harris, J. Phys.: Condens. Matter **10**, L215 (1998).

³ P.W. Anderson, Phys. Rev. **102**, 1008 (1956)

⁴ A. P. Ramirez, A. Hayashi, R.J. Cava, R. Siddharthan, and B.S. Shastry, Nature **399**, 333 (1999).

⁵ H. W. J. Blöte, R.F. Wielinga, and W. J. Huiskamp, Physica **43**, 549 (1969).

⁶ R. Siddharthan, B. S. Shastry, A. P. Ramirez, A. Hayashi, R. J. Cava, and S. Rosenkranz, Phys. Rev. Lett. **83**, 1854 (1999).

⁷ S. Rosenkranz, A. P. Ramirez, A. Hayashi, R. J. Cava, R. Siddharthan, and B. S. Shastry, J. Appl. Phys. **87**, 5914 (2000).

⁸ K. Matsuhira, Y. Hinatsu, K. Tenya, and T. Sakakibara, J. Phys.: Condens. Matter **12**, L649 (2000).

⁹ S. T. Bramwell, M. J. Harris, B. C. den Hertog, M. J. P. Gingras J. S. Gardner, D.F. McMorrow, A.R. Wildes, A.L. Cornelius, J. D. M. Champion, R. G. Melko, and T. Fen nell, cond-mat/0101114.

¹⁰ M. Kanada *et al.*, unpublished.

¹¹ B. C. den Hertog and M. J. P. Gingras, Phys. Rev. Lett. **84**, 3430 (2000).

¹² M. J. P. Gingras and B. C. den Hertog, cond-mat/0012275.

¹³ J. N. Reimers, J. E. Greedan, and M. Sato, J. Solid State Chem. **72**, 390 (1988).

¹⁴ F. Izumi, Chap. 13 of *The Rietveld Method*, edited by R. A. Young (Oxford Univ. Press, 1993).

¹⁵ W. Marshall and R. D. Lowde, Rep. Prog. Phys. **31**, 705 (1968).

¹⁶ S. W. Lovesey, *Theory of Neutron Scattering from Condensed Matter*, (Oxford Univ. Press, 1984).

¹⁷ J. N. Reimers, A. J. Berlinsky, and A.-C. Shi, Phys. Rev. B **43**, 865 (1991).

¹⁸ N. P. Raju, M. Dion, M. J. P. Gingras, T. E. Mason and J. E. Greedan, Phys. Rev. B **59**, 14489 (1999).

¹⁹ In a numerical calculation, slow convergence of the Fourier transform of the dipolar interaction has to be carefully treated. In the present work we carried out the summation of Eq. (4.4) in a large sphere of a radius $r = 10a$ or $20a$.

²⁰ This result is consistent with the mean field theory of Ref. 12, in which the Ising spin $\sigma_{n,\nu} = \pm 1$ is exactly treated in the Hamiltonian. In our approach the Ising spin is obtained by the limit $D_a \rightarrow \infty$. The ordered spin structure, which is not explicitly shown in Ref. 12, seems consistent with the present result.

²¹ R. G. Melko, B. C. den Hertog, and M. J. P. Gingras, cond-mat/0009225v2.

²² K. Motoya, S. M. Shapiro, and Y. Muraoka, Phys. Rev. B **28**, 6183 (1983).